Skeletal Radiology (2019) 48:119–127
https://doi.org/10.1007/s00256-018-3014-5

SCIENTIFIC ARTICLE

Imaging features of phosphaturic mesenchymal tumors

Stephen M. Broski[1] · Andrew L. Folpe[2] · Doris E. Wenger[1]

Received: 3 April 2018 / Revised: 11 June 2018 / Accepted: 17 June 2018 / Published online: 9 July 2018

Abstract

Objective To examine the CT and MR imaging features of phosphaturic mesenchymal tumors (PMTs).

Materials and methods With IRB approval, our institutional radiology/pathology database was reviewed for pathologically-proven PMTs. CT and MRI examinations were reviewed in consensus noting several imaging features, and if available, comparative molecular imaging tests were analyzed.

Results We identified 39 patients (21 male, 18 females) with 40 PMTs [mean age, 52.9 ± 14.9 years (range, 14–78)], including 20 bone and 20 soft tissue lesions. Mean maximal lesion diameter was 3.4 ± 2.0 cm (range, 1.1–9.8). 12/18 primary bone lesions (66.6%) were osteolytic and 15/20 (75.0%) had a narrow zone of transition. Internal matrix was present in 18/32 (56.3%) lesions. PMTs were most commonly T1 isointense (31/37, 83.8%), T2 hyperintense (14/36, 38.9%), and solidly enhancing (21/30, 70.0%). The majority (32/36, 88.9%) contained areas of dark T2 signal. 8/9 PMTs were positive by ^{99m}Tc-sestamibi scintigraphy, 2/4 by ^{111}In-pentetreotide scintigraphy, 2/2 by ^{68}Ga-DOTATATE PET/CT and 11/13 by ^{18}F-FDG PET/CT. On FDG PET/CT, the mean SUVmax was 4.1 ± 2.5 (range, 1.5–10.8).

Conclusions Osseous PMTs are commonly osteolytic with a narrow zone of transition. Both bone and soft tissue PMTs often contain matrix and areas of dark T2 signal on MRI, independent of the presence of matrix. However, PMTs may mimic other bone and soft tissue neoplasms, including fibrous dysplasia, tenosynovial giant cell tumor, and even atypical lipomatous tumor. As such, clinical presentation and laboratory correlation are critical to PMT recognition and accurate diagnosis.

Keywords PMT · Phosphaturic mesenchymal tumor · CT · MRI · PET/CT

Introduction

Tumor-induced osteomalacia (TIO), also called oncogenic osteomalacia, is a rare paraneoplastic condition characterized by renal phosphate wasting and osteomalacia due to tumor-secreted fibroblast growth factor-23 (FGF-23). Patients typically present with osteomalacia, bone pain, and proximal muscle weakness, with laboratory abnormalities including hypophosphatemia, hyperphosphaturia, normal serum calcium, and elevated serum FGF-23 levels [1]. The tumors producing FGF-23 are typically small and mesenchymal-derived, and their surgical removal results in reversal of the biochemical abnormalities.

The overwhelming majority of cases of TIO have been reported in association with a mesenchymal tumor of soft tissue or bone origin. Although McCance is usually credited for the first description of TIO [2], Prader was more likely the first to appreciate a neoplasm (described as a "giant cell reparative granuloma of bone") as the cause of his patient's symptoms [3]. Historically, it was felt that essentially any mesenchymal tumor type could cause TIO, with cases reported in association with highly vascular and/or matrix-producing tumors of bone and soft tissue [4, 5]. However, in 1972, Evans and Azzopardi observed that TIO-associated mesenchymal tumors might represent a unique tumor type [6] and in 1987, Weidner and Santa Cruz coined the term "phosphaturic mesenchymal tumor" (PMT) to describe these unusual neoplasms [7]. In 2004, Folpe and colleagues reviewed 32 cases of TIO and 108 previous published reports and found that over 90% of cases were due to a single histopathologic entity, phosphaturic mesenchymal tumor (PMT) [4]. This concept

✉ Doris E. Wenger
wenger.doris@mayo.edu

Stephen M. Broski
broski.stephen@mayo.edu

[1] Department of Radiology, Mayo Clinic, 200 First Street SW, Rochester, MN 55905, USA

[2] Department of Laboratory Medicine and Pathology, Mayo Clinic, 200 First Street SW, Rochester, MN 55905, USA

has been embraced by the World Health Organization in the 2013 Classification of Tumors of Soft Tissue and Bone, wherein PMTs are defined as "morphologically distinctive neoplasms that produce tumor-induced osteomalacia (TIO) in most affected patients, usually through production of fibroblast growth factor-23 (FGF-23)" [8]. Previous misclassification of PMT as other tumor types likely reflects their extreme rarity and lack of familiarity by pathologists with their morphological features.

Phosphaturic mesenchymal tumors (PMTs) may occur in the bones or soft tissues, including the subcutis [9], anywhere from the head to the toes. While typically benign, rare cases of malignant PMTs have been described [4, 10]. They are usually small and slow-growing, and for these reasons, classically difficult to localize. A variety of imaging techniques have been employed for diagnosis, including radiographs, CT, MRI, and various molecular imaging techniques. While several studies have detailed the use of functional imaging techniques such as ^{111}In-pentetreotide, ^{99}Tc-sestamibi, ^{18}F-FDG PET/CT, and ^{68}Ga-DOTATATE PET/CT [1, 11–25], there has been relatively less information regarding the CT and MRI features of these lesions, consisting solely of case reports or small series [1, 13, 26–31]. Therefore, we aimed to examine the CT and MR imaging features of PMTs, in order to elucidate any features that may aid in the detection and diagnosis of these rare tumors.

Materials and methods

With IRB approval, our radiology/pathology database was retrospectively reviewed for patients with pathologically proven PMTs between 1/1/1999 and 9/1/2017. Pathologic diagnosis was obtained by surgical resection or image-guided biopsy in all cases. Imaging modalities used for lesion evaluation were noted, including CT, MRI, and molecular imaging examinations. The electronic medical record was cross-referenced for relevant laboratory values obtained within the 6 months preceding pathologic confirmation and three months after surgical resection, if lesions were excised. A subset of patients was retrieved from a pathologic consultation database and did not have available laboratory data.

CT and MRI examinations were reviewed in consensus by two musculoskeletal radiologists. Lesion location and maximal lesion diameter were noted. CT characteristics evaluated included the presence and pattern of internal matrix (amorphous, punctate, or ground glass), pattern of osseous involvement (lytic, sclerotic, or mixed lytic/sclerotic), and zone of transition (wide or narrow). There was some heterogeneity in MRI protocols given varying lesion location and institution at which the MRI was performed, but at minimum, MRIs included fast spin echo (FSE) T1-weighted sequences (TR/TE, 400–900/minimum), FSE T2-weighted fat-suppressed sequences (TR/TE, 3000–5000/45–68), and either post-contrast fat-suppressed spoiled gradient recalled (TR/TE, 125–190/minimum) or fat-suppressed T1-weighted (TR/TE, 400–900/minimum) sequences. MRI characteristics evaluated included T1 signal intensity, T2 signal intensity, presence of internal fluid–fluid levels, intralesional hemorrhage, perilesional edema, and if contrast was given, the pattern of enhancement (solid, heterogeneous, or peripheral). The predominant lesional T1-weighted and T2-weighted fat-suppressed signal was compared to adjacent skeletal muscle to determine if lesions were hypointense, isointense, or hyperintense. Areas of signal intensity similar to adjacent cortical bone on T2-weighted, fat-suppressed images were defined as having dark, or low T2 signal. In primary bone lesions, the presence of transcortical extraosseous extension into the adjacent soft tissues was noted on both CT and MRI.

Molecular imaging examinations were assessed by a nuclear radiologist for the presence of radiotracer uptake in the lesion. Planar scintigraphy (^{99m}Tc-sestamibi, ^{111}In-pentetreotide, or ^{67}Ga-citrate) was considered positive if there was lesion uptake above adjacent background activity. FDG or DOTATATE PET/CTs were performed according to the standard institutional protocols. Weight and height were recorded for all patients. All patients undergoing FDG PET/CT had a blood glucose level of less than 200 mg/dl and were injected with 10–15 mCi of ^{18}F-FDG, with an incubation period of approximately 60 min. Patients undergoing ^{68}Ga-DOTATATE PET/CT were injected with 5.0–5.4 mCi. PET images were acquired with 2D or 3D ordered-subset expectation maximum, 128 × 128 matrix, and 3–5 min per bed position. Low-dose helical CT images were obtained for attenuation correction and anatomic localization. MIM software (MIM Software Inc., Cleveland, OH, USA) was used for PET/CT analysis. SUV values were determined by creating a volume of interest (VOI) incorporating the gross tumor volume. FDG PET/CT examinations were considered positive if the lesion had visually greater FDG activity than mediastinal blood pool. DOTATATE PET/CT examinations were considered positive if there was uptake constituting a Krenning score of ≥ 2.

Statistical analysis was performed using JMP software (JMP Pro, version 11.2.1, SAS Institute Inc.). Continuous variables are expressed as mean ± SD. Categorical variables are presented with absolute and relative frequencies. *P* values for between-group comparisons of continuous data were calculated from Kruskal–Wallis one-way analysis of variance (ANOVA). Statistical significance was established for p values of less than 0.05.

Results

In total, there were 39 patients (21 male, 18 females) with 40 PMTs. The average patient age was 52.9 ± 14.9 years of age (range, 14–78). Of the 40 lesions, 15 (37.5%) were located in

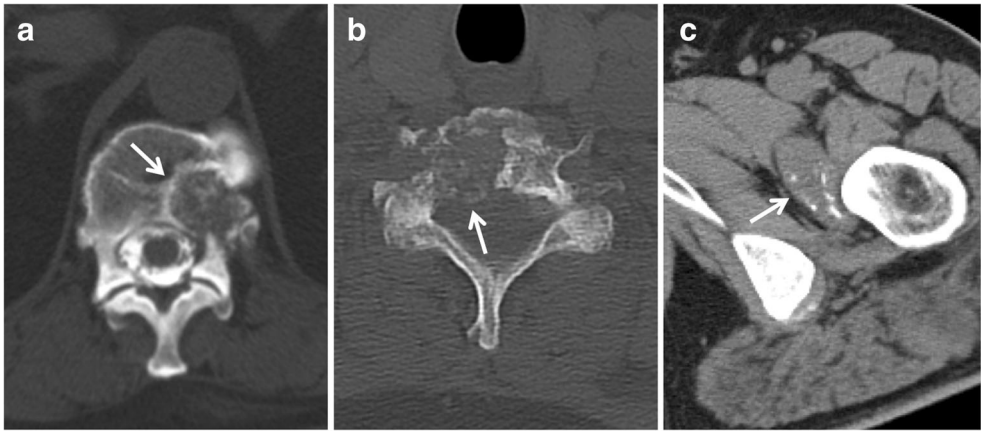

Fig. 1 A 73-year-old female with a PMT in the left T12 vertebral body (**a**, *arrow*), 60-year-old female with a PMT in the right C6 vertebral body (**b**, *arrow*), and a 61-year-old male with a PMT along the distal left iliopsoas tendon (**c**, *arrow*). The vertebral body lesions demonstrate amorphous matrix with a narrow zone of transition in **a** and wide zone of transition in **b**. The lesion in **c** shows punctate matrix

the lower extremity, seven (17.5%) in the head and neck region, six (15%) in the pelvis, six (15%) in the spine, three (7.5%) in the upper extremity, two (5%) in the thoracic trunk soft tissues, and one (2.5%) in a rib. There were 20 bone and 20 soft tissue lesions.

Twenty-seven of 40 lesions (67.5%) had correlative laboratory values obtained within the six months preceding imaging. Nineteen of 27 patients had abnormal phosphorus levels, 17 of which were hypophosphatemic, with an average level of 2.1 ± 0.99 mg/dl (range, 1.1–5.5; normal value, 2.5–4.5). Sixteen of 19 patients had elevated total alkaline phosphatase (AP) levels, with average total AP of 240.1 ± 143.58 U/l (range, 63–658; normal value, 45–118). In patients with a bone-specific AP fraction, 8/12 were elevated, with an average level of 48.0 ± 32.2 U/l (range, 11–104; normal value, 0–20); 9/17 patients had elevated parathyroid hormone levels (112.1 ± 108.5 pg/ml, range, 27–462; normal value, 15–65), while 12/17 patients had elevated serum FGF23 levels (1686.5 RU/ml ± 5211.6, range, undetectable - 20,500; normal value, < 180).

Twelve of 40 lesions (30%) were FGF-23 positive by chromogenic in situ hybridization (CISH), and 11/40 (27.5%) were FGF-23 positive by reverse transcription polymerase chain reaction (RT-PCR). Of the remaining 17 cases, seven patients had elevated serum FGF-23 levels, six had typical laboratory findings of TIO (including hypophosphatemia) that normalized after surgical resection, and two patients had normal phosphorous levels in the setting of tertiary hyperparathyroidism and also had laboratory normalization after resection.

Thirty-two (80.0%) lesions had CT evaluation, while 37/40 (92.5%) had MRI evaluation. Twenty-three lesions (57.5%) had molecular imaging evaluation, including ^{99m}Tc-sestamibi scintigraphy (nine), ^{111}In-pentetreotide scintigraphy (four), ^{67}Ga-citrate scintigraphy (one), ^{18}F-FDG PET/CT (13), and ^{68}Ga-DOTATATE PET/CT (two), with some patients having more than one type of molecular imaging test.

The mean maximal lesion diameter was 3.4 ± 2.0 cm (range, 1.1–9.8). Internal matrix was present in 18/32 (56.3%) lesions (Fig. 1), including 7/32 (21.9%) with amorphous, 8/32 (25%) with punctate, and 3/32 (9.4%) with ground glass character. This was more common in osseous lesions (13/18, 72.2%) than soft tissue lesions (5/14, 35.7.6%), but the difference was not statistically significant ($p = 0.072$). A minority of bone lesions demonstrated an extraosseous soft tissue component (5/20, 25.0%), and on CT, 15/18 primary bone lesions (83.3%) were osteolytic, 1/18 (5.6%) was osteosclerotic, and 2/18 (11.1%) were mixed osteolytic/osteosclerotic. The majority of osseous lesions (15/20, 75.0%) had a narrow zone of transition, while 5/20 (25.0%) had a wide zone of transition.

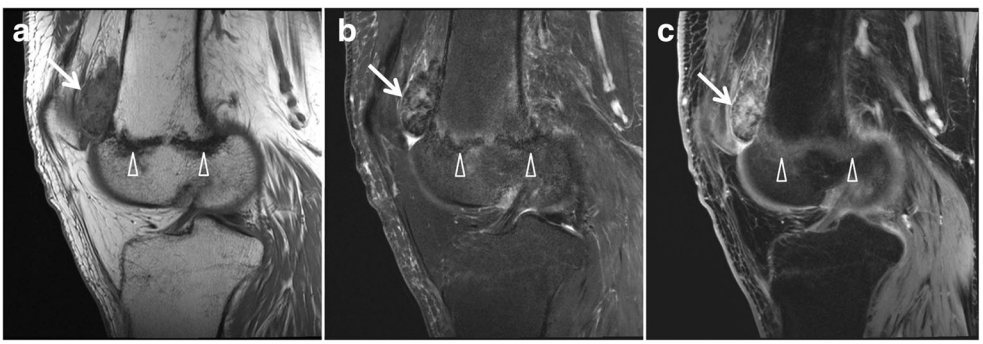

Fig. 2 A 71-year-old male with a PMT in the left prefemoral fat pad. The lesion demonstrates heterogeneous isointense signal on T1-weighted (**a**, *arrow*), heterogeneous hypointense signal on T2-weighted fat-saturated (**b**, *arrow*) images and heterogeneous enhancement (**c**, *arrow*) mimicking a tenosynovial giant cell tumor. Note the insufficiency-type stress fracture in the distal left femur (*arrowheads*)

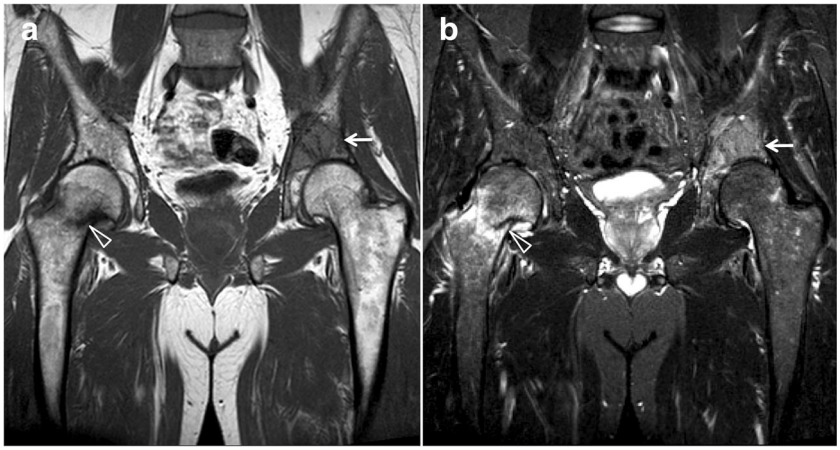

Fig. 3 A 49-year-old male with a left acetabular PMT. Coronal MRI images demonstrate increased T1 (**a**, *arrow*) and T2 signal relative to skeletal muscle with areas of superimposed T2 hypointensity (**b**, *arrow*) within the lesion, and an incomplete insufficiency-type stress fracture in the medial right femoral neck (*arrowheads*)

On MRI evaluation, the majority of lesions (31/37, 83.8%) demonstrated intermediate T1 signal, while 3/37 (8.1%) were heterogeneous, 2/37 (5.4%) were hyperintense, and 1/37 (2.7%) was hypointense. The predominant T2-weighted signal in these lesions varied from hyperintense (14/36, 38.9%), to intermediate (9/36, 25.0%), hypointense (4/36, 11.1%), and heterogeneous (9/36, 25.0%). However, the vast majority of cases (32/36, 88.9%) contained areas of dark T2 signal (Fig. 2), even if the dominant lesion signal intensity was T2 hyperintense. This was independent of the presence of internal matrix ($p = 0.23$). Four of 37 lesions (10.8%) exhibited internal fluid–fluid levels, 4/37 lesions (10.8%) demonstrated internal hemorrhage, and 3/37 (8.1%) lesions had perilesional edema. Thirty of 37 MRI examinations were performed with IV gadolinium-based contrast, and 21/30 (70.0%) lesions had solid enhancement, 7/30 (23.3%) demonstrated heterogeneous enhancement, and 2/30 (6.7%) had peripheral enhancement. After excluding head and neck lesions evaluated by head CT or brain MRI, 14 of the remaining 33 lesions (42.4%) had a fracture visible on the same MRI or CT in which the primary PMT was visible (Figs. 2 and 3).

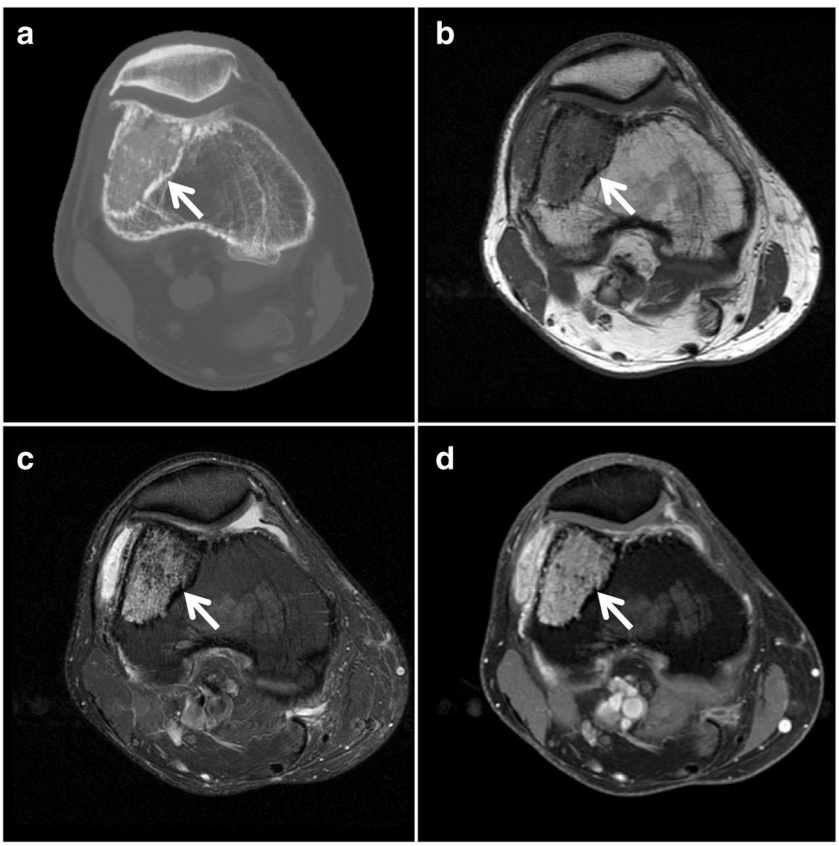

Fig. 4 A 53-year-old male with a PMT in the distal right femur. Axial CT and MRI images demonstrate internal ground glass matrix and a thin sclerotic rim (**a**, *arrow*), T1 isointensity (**b**, *arrow*), heterogeneous T2 hyperintensity with areas of low T2 signal (**c**, *arrow*), and solid enhancement (**d**, *arrow*). The differential diagnosis would include fibrous dysplasia

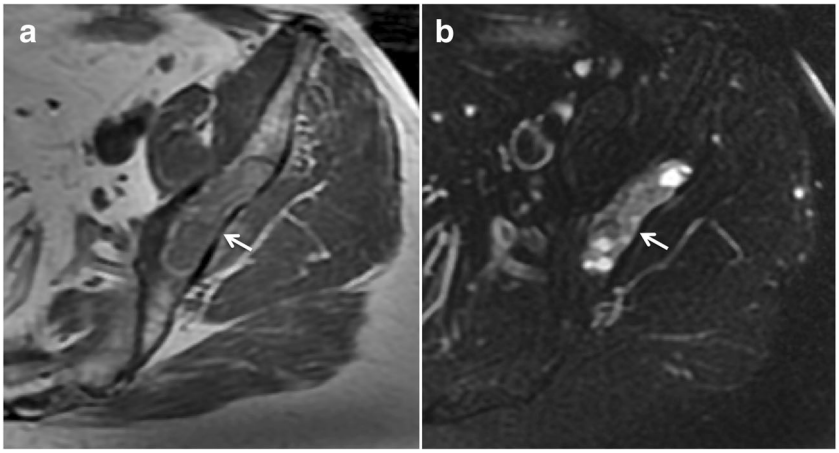

Fig. 5 A 47-year-old male with a left iliac bone PMT. Axial MRI images demonstrate a T1 isointense lesion with a thin rim of T1 hyperintensity (**a**, *arrow*), and heterogeneous predominantly low T2 signal (**b**, *arrow*) mimicking fibrous dysplasia

Nine lesions underwent evaluation by ^{99m}Tc-sestamibi scintigraphy, four with ^{111}In-pentetreotide scintigraphy, one with ^{67}Ga-citrate scintigraphy, 13 with ^{18}F-FDG PET/CT, and two with ^{68}Ga-DOTATATE PET/CT. Eight of the nine lesions were positive on ^{99m}Tc-sestamibi, 2/4 were positive with ^{111}In-pentetreotide scintigraphy, and one lesion evaluated by ^{67}Ga-citrate scintigraphy demonstrated no uptake. Using blood pool SUVmax as the threshold for positivity, 11/13 lesions (84.6%) were positive by ^{18}F-FDG PET/CT. Both lesions evaluated by ^{68}Ga-DOTATATE PET/CT were positive, demonstrating intense uptake greater than that of the spleen. On FDG PET/CT, the mean SUVmax was 4.1 ± 2.5 (range, 1.5–10.8), while on DOTATATE PET/CT the mean SUVmax was 14.1 ±/6.7 (range, 9.3–18.8).

Discussion

To the best of our knowledge, this study represents the largest published series to date examining the CT and MRI features of pathologically proven phosphaturic mesenchymal tumors. Our results confirm the variable location and small size of

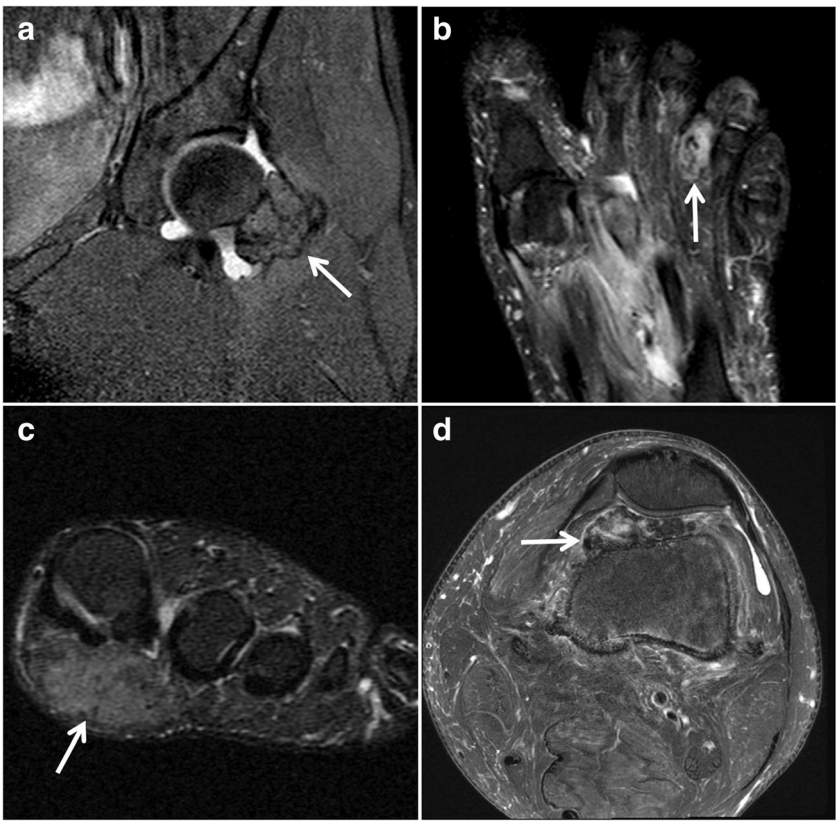

Fig. 6 Examples of PMTs with an imaging appearance mimicking T2 hypointense tenosynovial giant cell tumors on fat-suppressed fluid-sensitive sequences, including an intra-articular lesion involving the left hip in a 38-year-old female (**a**, *arrow*), in the soft tissues of the left 4th toe in a 57-year-old male (**b**, *arrow*), along the plantar aspect of the left first toe flexor tendon in a 60-year-old female (**c**, *arrow*), and in the left prefemoral fat pad in a 71-year-old male (**d**, *arrow*)

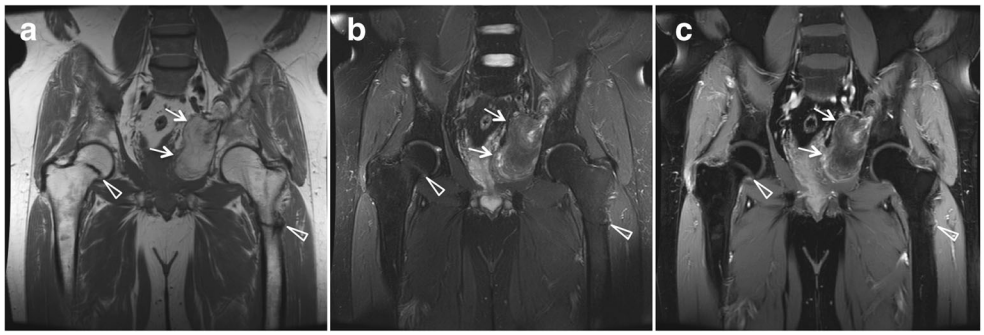

Fig. 7 A 58-year-old male with an extraperitoneal PMT in the left pelvis. Coronal T1-weighted (**a**), T2-weighted fat-saturated (**b**), and post-gadolinium fat-saturated spoiled gradient recalled (**c**) images demonstrate a mass comprised predominantly of fat, with interspersed areas of hazy non-lipomatous signal, mimicking an atypical lipomatous tumor (*arrows*). Note the insufficiency-type stress fractures in the subcapital region of the right femoral neck and subtrochanteric region of the left femur (*arrowheads*)

these tumors (average maximal diameter 3.4 ± 2.0 cm). A unique feature best demonstrated on CT was the presence of internal matrix, found in just over half of our patients. This matrix was most often punctate (8/32, 25.0%) or amorphous (7/32, 21.9%), and less commonly ground glass (3/32, 9.4%). This likely correlates with the "grungy" or flocculent pattern of PMT matrix calcification often described histopathologically [4, 7, 32]. Bone lesions were most commonly osteolytic with a narrow zone of transition. On MRI, the overwhelming majority of lesions demonstrated intermediate T1 signal. Although the T2 signal intensity was more variable, the majority of lesions were T2 hyperintense. However, a defining feature on MRI was the presence of foci of dark signal on T2-weighted fat-suppressed images (32/36, 88.9%), even if the predominant signal intensity was T2 hyperintense. This was also found to be independent of the presence of internal matrix. Examples of phosphaturic mesenchymal tumors with areas of low signal intensity on T2-weighted MRI images have been reported in several previous studies [26, 33, 34], so this seems to be a relatively constant imaging feature. It was also common to identify insufficiency-type stress fractures on the imaging studies obtained to localize the PMT in these patients, including both CT and MRI. Therefore, even without adequate clinical information, the presence of a stress fracture in conjunction with a bone or soft tissue tumor, especially in a younger patient without other risk factors for osteoporosis or osteomalacia, may be an important clue to the diagnosis of PMT.

Despite these trends, the imaging features of PMTs are variable and can simulate other more common bone and soft tissue neoplasms, and it is evident why this lesion has often been misdiagnosed. For example, bone lesions with ground glass attenuation and thin sclerotic rim on CT (Fig. 4) or with heterogeneous but predominantly low T2 signal intensity on MRI (Fig. 5) may mimic fibrous dysplasia. Lesions with predominant low T2 signal within or along joints and tendon sheaths mimic focal-type tenosynovial giant cell tumors

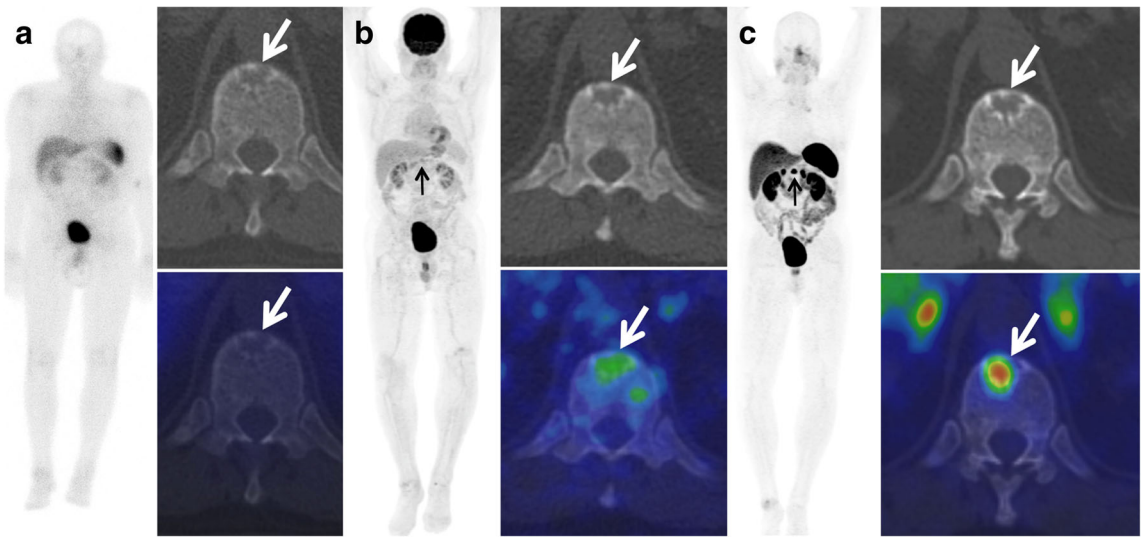

Fig. 8 A 70-year-old male with a PMT in the T11 vertebral body. The tumor shows no significant pentetreotide uptake (**a**, *arrows*), low-grade FDG activity (**b**, *arrows*), and intense DOTATATE uptake (**c**, *arrows*). On CT, it is osteolytic with a thin sclerotic rim, and was morphologically stable over many years, mimicking an atypical vertebral body hemangioma

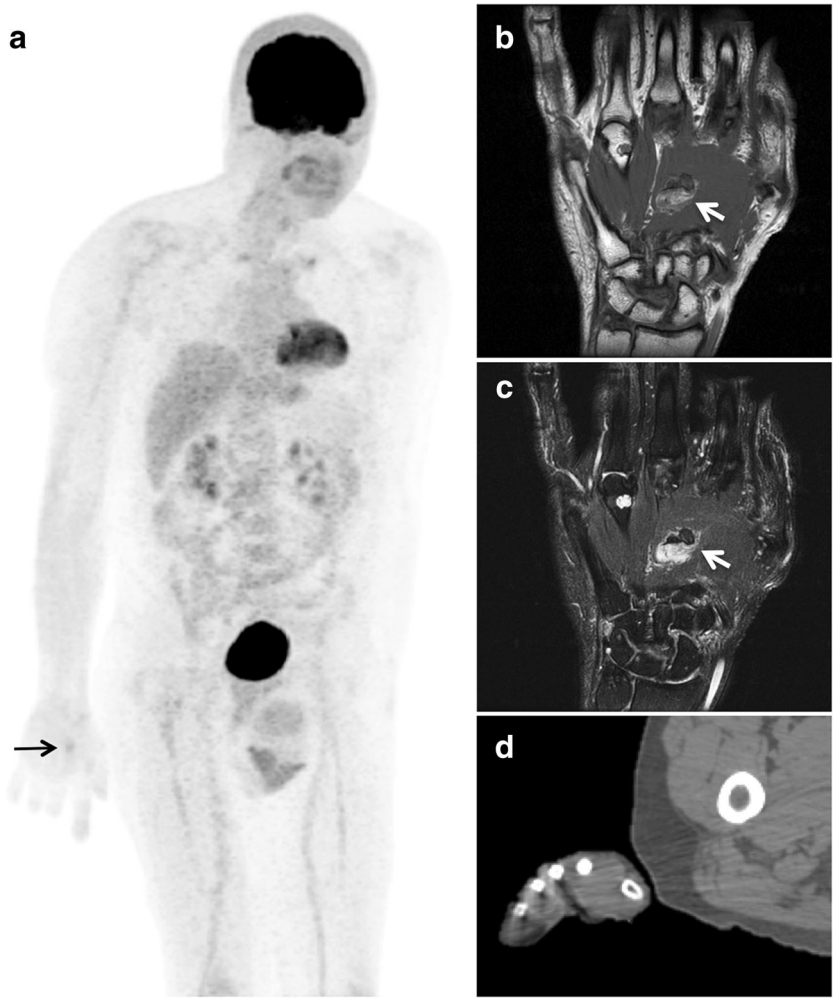

Fig. 9 A 56-year-old male with a PMT in the palmar soft tissues of the right hand. FDG PET/CT shows low-grade activity (SUVmax 2.4) within the lesion (**a**, *arrow*). On MRI, the lesion demonstrates heterogeneous T1 (**b**, *arrow*) and T2 signal (**c**, *arrow*), with areas of prominent dark T2 signal (**c**). There was no corresponding internal matrix on the CT images from PET/CT (**d**). This case highlights the importance of including the extremities when imaging patients with tumor-induced osteomalacia

(Fig. 6). Lastly, we present the first case in the literature with a predominant fatty component, mimicking an atypical lipomatous tumor (Fig. 7).

PMTs variably express five somatostatin receptors (SSTR1–5), and uniform expression of the SSTR2A subtype has been recently demonstrated in multiple studies [35, 36]. Their somatostatin avidity has been exploited to image these tumors with somatostatin-analogues, including ^{111}In-pentetreotide [14, 16–20]. More recently, ^{68}Ga-DOTATATE and other ^{68}Ga-DOTA PET agents have been used with

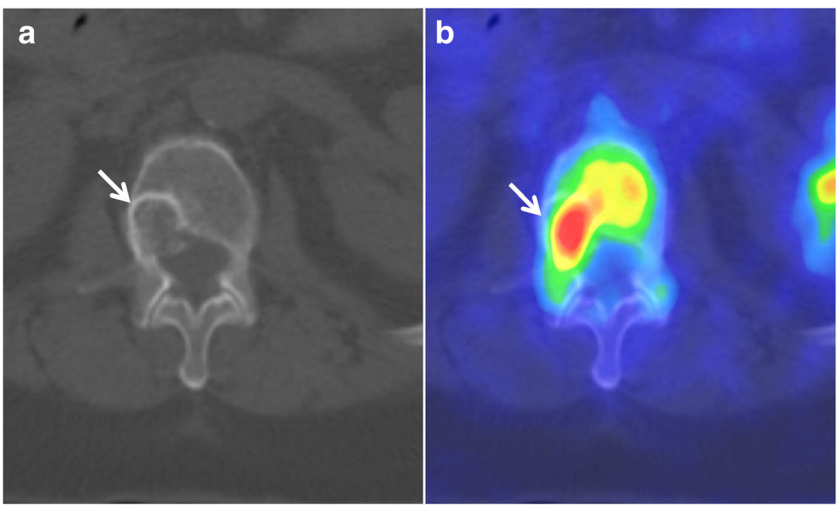

Fig. 10 A 68-year-old female with a PMT in the right L2 vertebral body. Axial CT (**a**) and fused FDG PET/CT (**b**) images demonstrate an osteolytic lesion with a thin sclerotic rim, internal amorphous matrix, and intense FDG activity with an SUVmax of 10.8 (*arrows*)

success to localize PMTs [15], to better advantage than ^{111}In-pentetreotide scintigraphy [37] and FDG PET/CT [11, 14], which we found exemplified in at least one instance in our small cohort (Fig. 8). While ^{68}Ga-DOTATATE has recently become FDA approved for the evaluation of neuroendocrine tumors, its use for imaging PMTs is off-label, and therefore FDG PET/CT may remain a useful tool in the imaging algorithm of PMTs until the widespread clinical availability of ^{68}Ga-DOTATATE and approval of its use in evaluating TIO. FDG PET/CT has been shown to be useful in PMT evaluation in multiple studies [14, 23, 24, 30, 38]. The results from the 13 patients who underwent FDG PET/CT in our cohort represent a significant contribution to the available literature detailing the role of FDG PET/CT in PMT imaging evaluation. We found that while the metabolic activity may be variable (Figs. 9 and 10), with uptake ranging from below blood pool to intense (SUVmax 1.5–10.1), these lesions are most often moderately FDG-avid (mean SUVmax 4.1 ± 2.5), in concordance with prior reports. Given the variable location, whole-body imaging with inclusion of the distal extremities (Fig. 9) should be prescribed in patients with TIO in which the primary PMT has not been localized.

Despite the clear role for whole-body functional imaging techniques, whole-body MRI has also been advocated for PMT localization [31]. Further, most if not all lesions detected by whole-body imaging will require focused anatomic assessment with MRI and/or CT for preoperative planning. Therefore, it is important to be aware of the most common CT and MRI features of these tumors to aid in diagnosis and detection, including the frequency of internal matrix and areas of T2 hypointensity. Perhaps most critical is a recognition of how closely these tumors may mimic other benign and malignant bone and soft tissue lesions when generating a differential diagnosis. The clinical context is paramount in these patients and correlation with typical laboratory features including hypophosphatemia, elevated alkaline phosphatase, and elevated systemic FGF-23 levels is recommended. Recognition of osteomalacia is also important, which may manifest on MRI and CT as the presence of insufficiency-type stress fractures. However, several reports exist of pathologically confirmed PMTs (FGF-23 positivity confirmed by either CISH or RT-PCR) in patients without TIO [32, 39], and so typical laboratory abnormalities are not an absolute prerequisite to make the diagnosis.

This study had several limitations, including its small size and retrospective nature. CT and MRI studies were not available in every single PMT case, and there was heterogeneity amongst the various MRI protocols used to evaluate the patients. Further studies and/or pooled data from multiple centers could be helpful to further elucidate the typical CT and MRI findings of this very rare tumor.

Conclusions

The majority of osseous PMTs are osteolytic with a narrow zone of transition on CT. Both bone and soft tissue PMTs commonly contain matrix and areas of dark T2 signal on MRI, independent of the presence of matrix. However, PMTs may mimic other bone and soft tissue neoplasms, including fibrous dysplasia, tenosynovial giant cell tumor, and even atypical lipomatous tumor. As such, clinical presentation and laboratory correlation are critical to PMT recognition and accurate diagnosis.

Compliance with ethical standards

Conflict of interest The authors declare that they have no conflicts of interest.

Ethical approval All procedures performed in studies involving human participants were in accordance with the ethical standards of the institutional and/or national research committee and with the 1964 Helsinki Declaration and its later amendments or comparable ethical standards.

Informed consent The need for informed consent was waived by the Institutional Review Board.

References

1. Kumar R, Folpe AL, Mullan BP. Tumor-induced osteomalacia. Transl Endocrinol Metab 2015;7(3):1871.
2. McCance RA. Osteomalacia with Looser's nodes (Milkman's syndrome) due to a raised resistance to vitamin D acquired about the age of 15 years. Q J Med. 1947;16:33–46.
3. Prader A, Illig R, Uehlinger RE, Stalder G. Rachitis infolge knochentumors (rickets caused by bone tumors). Helv Pediatr Acta. 1959;14:554–65.
4. Folpe AL, Fanburg-Smith JC, Billings SD, Bisceglia M, Bertoni F, Cho JY, et al. Most osteomalacia-associated mesenchymal tumors are a single histopathologic entity: an analysis of 32 cases and a comprehensive review of the literature. Am J Surg Pathol. 2004;28(1):1–30.
5. Sundaram M, McCarthy EF. Oncogenic osteomalacia. Skelet Radiol. 2000;29(3):117–24.
6. Evans DJ, Azzopardi JG. Distinctive tumours of bone and soft tissue causing acquired vitamin-D-resistant osteomalacia. Lancet. 1972;1(7746):353–4.
7. Weidner N, Santa Cruz D. Phosphaturic mesenchymal tumors. A polymorphous group causing osteomalacia or rickets. Cancer. 1987;59(8):1442–54.
8. CDM F. WHO classification of tumours of soft tissue and bone. Lyon: IARC Press; 2013.
9. Gardner KH, Shon W, Folpe AL, Wieland CN, Tebben PJ, Baum CL. Tumor-induced osteomalacia resulting from primary cutaneous phosphaturic mesenchymal tumor: a case and review of the medical literature. J Cutan Pathol. 2013;40(9):780–4. quiz 779
10. Woo VL, Landesberg R, Imel EA, Singer SR, Folpe AL, Econs MJ, et al. Phosphaturic mesenchymal tumor, mixed connective tissue variant, of the mandible: report of a case and review of the literature. Oral Surg Oral Med Oral Pathol Oral Radiol Endod. 2009;108(6):925–32.

11. Agrawal K, Bhadada S, Mittal BR, Shukla J, Sood A, Bhattacharya A, et al. Comparison of 18F-FDG and 68Ga DOTATATE PET/CT in localization of tumor causing oncogenic osteomalacia. Clin Nucl Med. 2015;40(1):e6–e10.
12. Clifton-Bligh RJ, Hofman MS, Duncan E, Sim Ie W, Darnell D, Clarkson A, et al. Improving diagnosis of tumor-induced osteomalacia with Gallium-68 DOTATATE PET/CT. J Clin Endocrinol Metab. 2013;98(2):687–94.
13. Ho CL. Ga68-DOTA peptide PET/CT to detect occult mesenchymal tumor-inducing osteomalacia: a case series of three patients. Nucl Med Mol Imaging. 2015;49(3):231–6.
14. Jadhav S, Kasaliwal R, Lele V, Rangarajan V, Chandra P, Shah H, et al. Functional imaging in primary tumour-induced osteomalacia: relative performance of FDG PET/CT vs somatostatin receptor-based functional scans: a series of nine patients. Clin Endocrinol. 2014;81(1):31–7.
15. Zhang J, Zhu Z, Zhong D, Dang Y, Xing H, Du Y, et al. 68Ga DOTATATE PET/CT is an accurate imaging modality in the detection of culprit tumors causing osteomalacia. Clin Nucl Med. 2015;40(8):642–6.
16. Duet M, Kerkeni S, Sfar R, Bazille C, Liote F, Orcel P. Clinical impact of somatostatin receptor scintigraphy in the management of tumor-induced osteomalacia. Clin Nucl Med. 2008;33(11):752–6.
17. Garcia CA, Spencer RP. Bone and In-111 octreotide imaging in oncogenic osteomalacia: a case report. Clin Nucl Med. 2002;27(8):582–3.
18. Jan de Beur SM, Streeten EA, Civelek AC, McCarthy EF, Uribe L, Marx SJ, et al. Localisation of mesenchymal tumours by somatostatin receptor imaging. Lancet. 2002;359(9308):761–3.
19. Nguyen BD, Wang EA. Indium-111 pentetreotide scintigraphy of mesenchymal tumor with oncogenic osteomalacia. Clin Nucl Med. 1999;24(2):130–1.
20. Rhee Y, Lee JD, Shin KH, Lee HC, Huh KB, Lim SK. Oncogenic osteomalacia associated with mesenchymal tumour detected by indium-111 octreotide scintigraphy. Clin Endocrinol. 2001;54(4):551–4.
21. Chong WH, Andreopoulou P, Chen CC, Reynolds J, Guthrie L, Kelly M, et al. Tumor localization and biochemical response to cure in tumor-induced osteomalacia. J Bone Miner Res. 2013;28(6):1386–98.
22. Hodgson SF, Clarke BL, Tebben PJ, Mullan BP, Cooney WP 3rd, Shives TC. Oncogenic osteomalacia: localization of underlying peripheral mesenchymal tumors with use of Tc 99m sestamibi scintigraphy. Endocr Pract. 2006;12(1):35–42.
23. Andreopoulou P, Dumitrescu CE, Kelly MH, Brillante BA, Cutler Peck CM, Wodajo FM, et al. Selective venous catheterization for the localization of phosphaturic mesenchymal tumors. J Bone Miner Res. 2011;26(6):1295–302.
24. Dupond JL, Mahammedi H, Prie D, Collin F, Gil H, Blagosklonov O, et al. Oncogenic osteomalacia: diagnostic importance of fibroblast growth factor 23 and F-18 fluorodeoxyglucose PET/CT scan for the diagnosis and follow-up in one case. Bone. 2005;36(3):375–8.
25. Jiang Y, Xia WB, Xing XP, Silva BC, Li M, Wang O, et al. Tumor-induced osteomalacia: an important cause of adult-onset hypophosphatemic osteomalacia in China: report of 39 cases and review of the literature. J Bone Miner Res. 2012;27(9):1967–75.
26. Koplas MC, Rubin BP, Sundaram M. Phosphaturic mesenchymal tumor: two contrasting cases. Skelet Radiol. 2014;43(6):841–5.
27. Nakanishi K, Sakai M, Tanaka H, Tsuboi H, Hashimoto J, Hashimoto N, et al. Whole-body MR imaging in detecting phosphaturic mesenchymal tumor (PMT) in tumor-induced hypophosphatemic osteomalacia. Magn Reson Med Sci. 2013;12(1):47–52.
28. Avila NA, Skarulis M, Rubino DM, Doppman JL. Oncogenic osteomalacia: lesion detection by MR skeletal survey. AJR Am J Roentgenol. 1996;167(2):343–5.
29. Nelson AE, Mason RS, Robinson BG, Hogan JJ, Martin EA, Ahlstrom H, et al. Diagnosis of a patient with oncogenic osteomalacia using a phosphate uptake bioassay of serum and magnetic resonance imaging. Eur J Endocrinol. 2001;145(4):469–76.
30. Seo HJ, Choi YJ, Kim HJ, Jeong YH, Cho A, Lee JH, et al. Using (18)F-FDG PET/CT to detect an occult mesenchymal tumor causing oncogenic osteomalacia. Nucl Med Mol Imaging. 2011;45(3):233–7.
31. Dissanayake AM, Wilson JL, Holdaway IM, Reid IR. Oncogenic osteomalacia: culprit tumour detection whole-body magnetic resonance imaging. Intern Med J. 2003;33(12):615–6.
32. Bahrami A, Weiss SW, Montgomery E, Horvai AE, Jin L, Inwards CY, et al. RT-PCR analysis for FGF23 using paraffin sections in the diagnosis of phosphaturic mesenchymal tumors with and without known tumor induced osteomalacia. Am J Surg Pathol. 2009;33(9):1348–54.
33. Flanagan AM, Delaney D, O'Donnell P. Benefits of molecular pathology in the diagnosis of musculoskeletal disease: part II of a two-part review: bone tumors and metabolic disorders. Skelet Radiol. 2010;39(3):213–24.
34. Slot-Steenks MM, Hamdy NA, van de Sande MA, Vriens D, Cleven AH, Appelman-Dijkstra NM. Identifying the culprit lesion in tumor induced hypophosphatemia, the solution of a clinical enigma. Endocrine. 2016;54(3):642–7.
35. Agaimy A, Michal M, Chiosea S, Petersson F, Hadravsky L, Kristiansen G, et al. Phosphaturic mesenchymal tumors: clinicopathologic, immunohistochemical and molecular analysis of 22 cases expanding their morphologic and immunophenotypic spectrum. Am J Surg Pathol. 2017;41(10):1371–80.
36. Houang M, Clarkson A, Sioson L, Elston MS, Clifton-Bligh RJ, Dray M, et al. Phosphaturic mesenchymal tumors show positive staining for somatostatin receptor 2A (SSTR2A). Hum Pathol. 2013;44(12):2711–8.
37. Breer S, Brunkhorst T, Beil FT, Peldschus K, Heiland M, Klutmann S, et al. 68Ga DOTA-TATE PET/CT allows tumor localization in patients with tumor-induced osteomalacia but negative 111In-octreotide SPECT/CT. Bone. 2014;64:222–7.
38. Jagtap VS, Sarathi V, Lila AR, Malhotra G, Sankhe SS, Bandgar T, et al. Tumor-induced osteomalacia: a single center experience. Endocr Pract. 2011;17(2):177–84.
39. Sent-Doux KN, Mackinnon C, Lee JC, Folpe AL, Habeeb O. Phosphaturic mesenchymal tumor without osteomalacia: additional confirmation of the "non-phosphaturic" variant, with emphasis on the roles of FGF23 chromogenic in situ hybridization and FN1-FGFR1 fluorescence in situ hybridization. Hum Pathol. 2018. https://doi.org/10.1016/j.humpath.2018.02.022.